EVPA Swing Mechanisms in AGN Jets:
stochastic vs. deterministic

The Quasar Movie Project

by Sebastian Kiehlmann
on behalf of the Quasar Movie Project team
PI: Dr. Tuomas Savolainen

Max Planck Institute for Radio Astronomy,
Auf dem Hügel 69, 53121 Bonn, Germany

MAX-PLANCK-GESELLSCHAFT

IMPRS astronomy & astrophysics Bonn and Cologne

Outlook

i. Introduction:
   AGN jets and EVPA swings

ii. Random walks
    in Stokes-Q-U-space

iii. EVPA swing mechanisms

iv. Helical motion model

I. Introduction:

AGN Jets

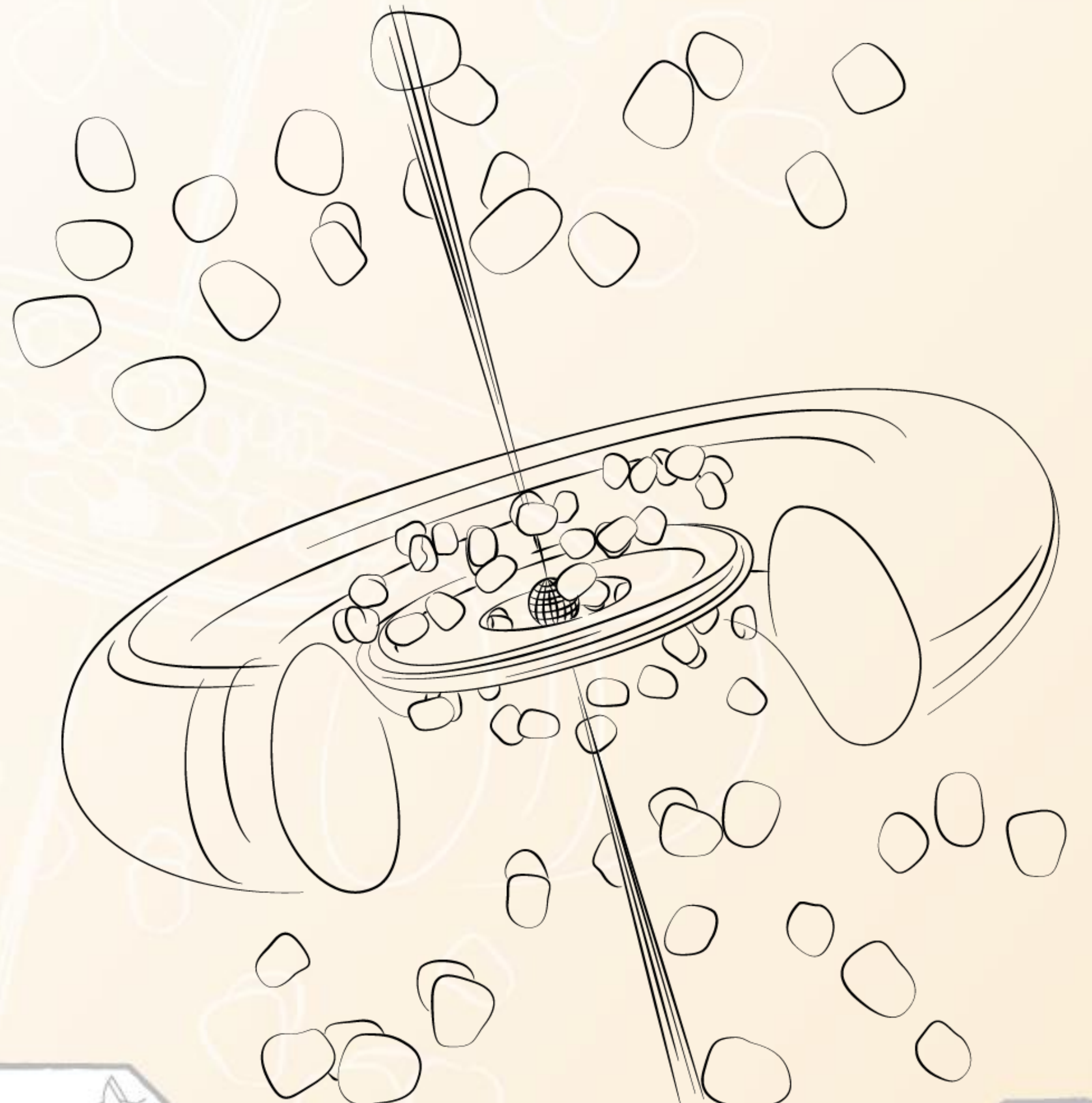

Fig. 1: Sketched
Active **G**alactic **N**ucleus

SEBASTIAN KIEHLMANN, DIPL.-PHYS.
MAX-PLANCK INSTITUT FÜR RADIOASTRONOMIE, BONN

I. Introduction:

AGN Jets

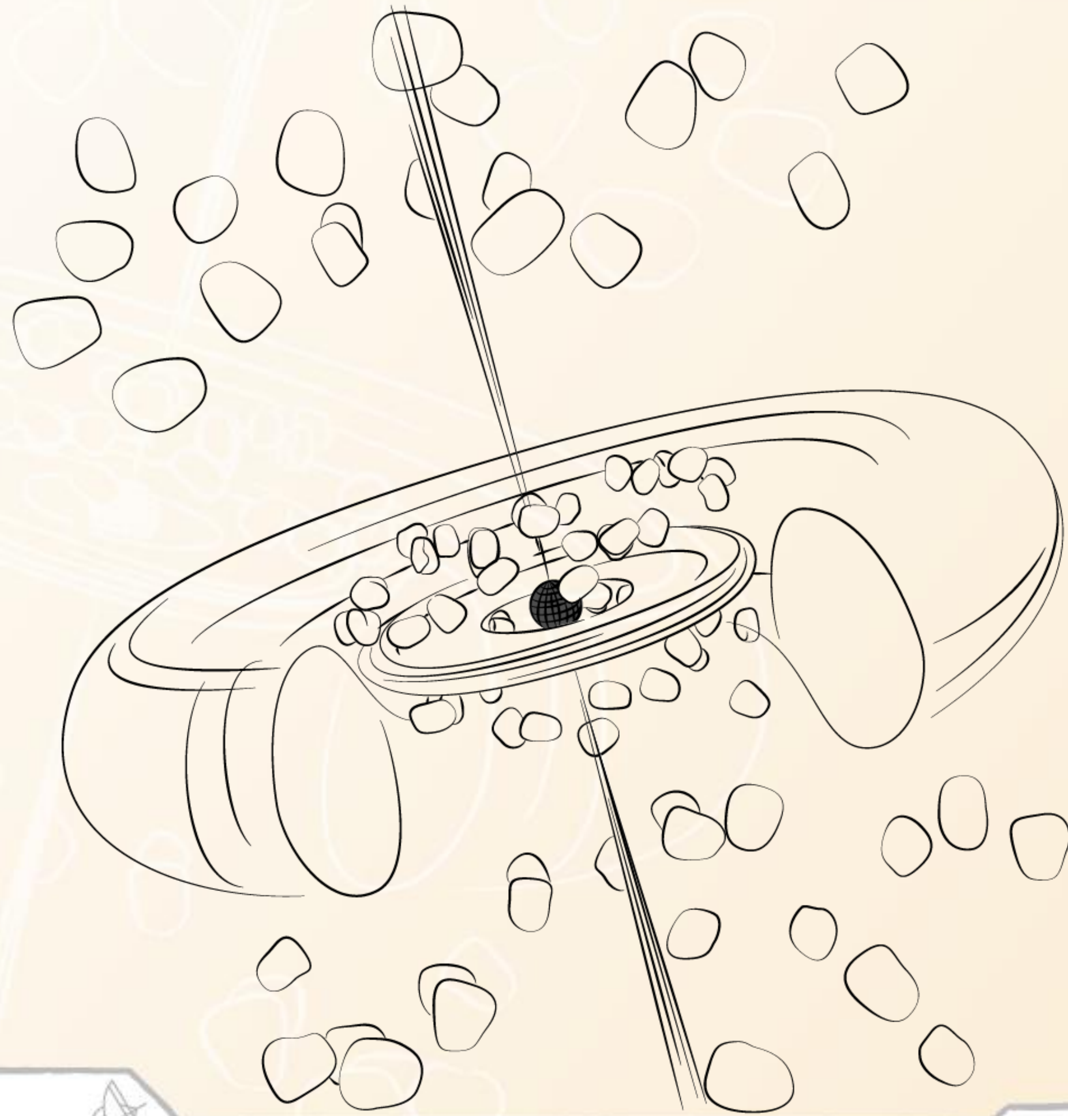

Fig. 1: Sketched
Active **G**alactic **N**ucleus

SEBASTIAN KIEHLMANN, DIPL.-PHYS.
MAX-PLANCK INSTITUT FÜR RADIOASTRONOMIE, BONN

I. Introduction:

AGN Jets

Fig. 1: Sketched
Active **G**alactic **N**ucleus

SEBASTIAN KIEHLMANN, DIPL.-PHYS.
MAX-PLANCK INSTITUT FÜR RADIOASTRONOMIE, BONN

I. Introduction:

AGN Jets

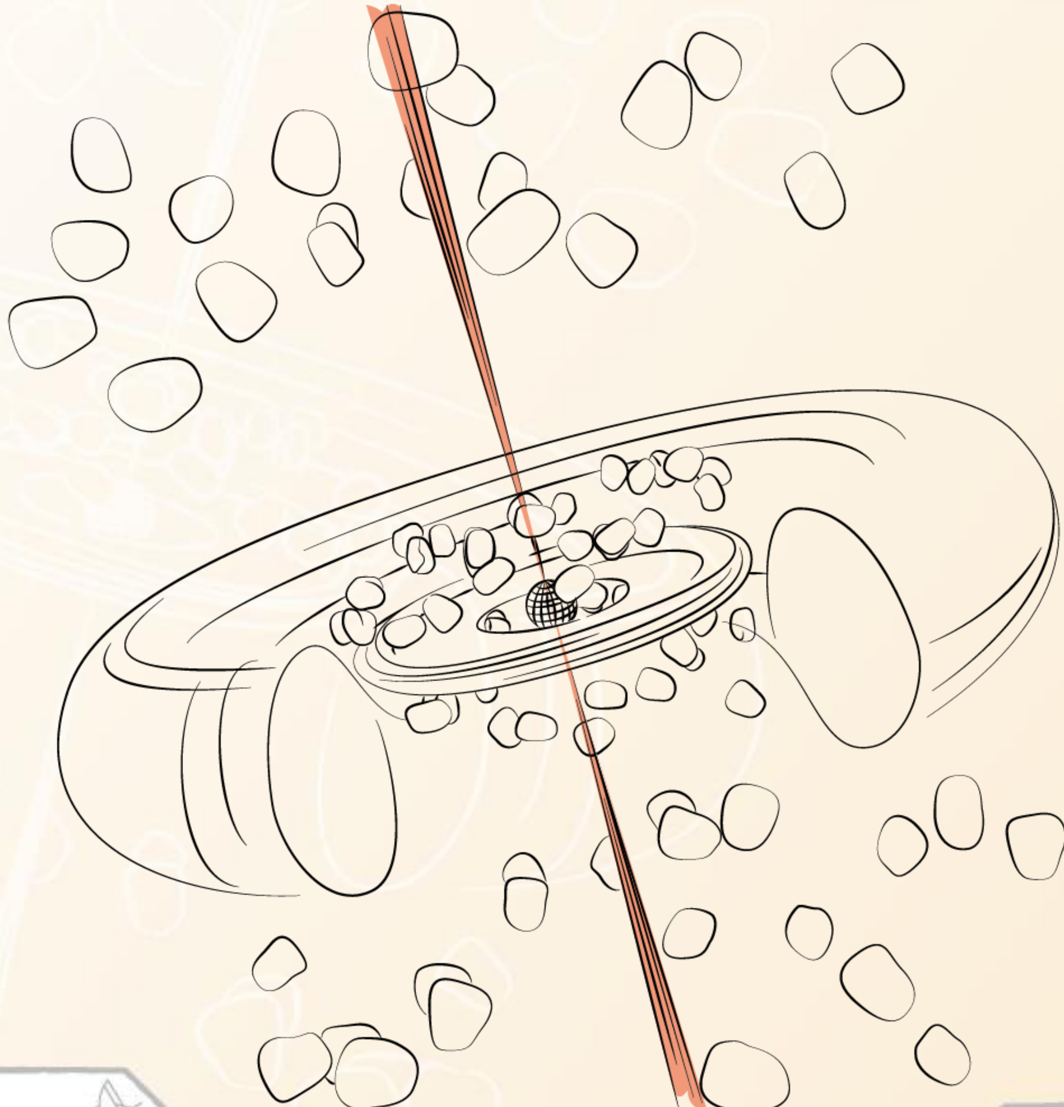

Fig. 1: Sketched
Active **G**alactic **N**ucleus

SEBASTIAN KIEHLMANN, DIPL.-PHYS.
MAX-PLANCK INSTITUT FÜR RADIOASTRONOMIE, BONN

I. Introduction:

Blazar SED

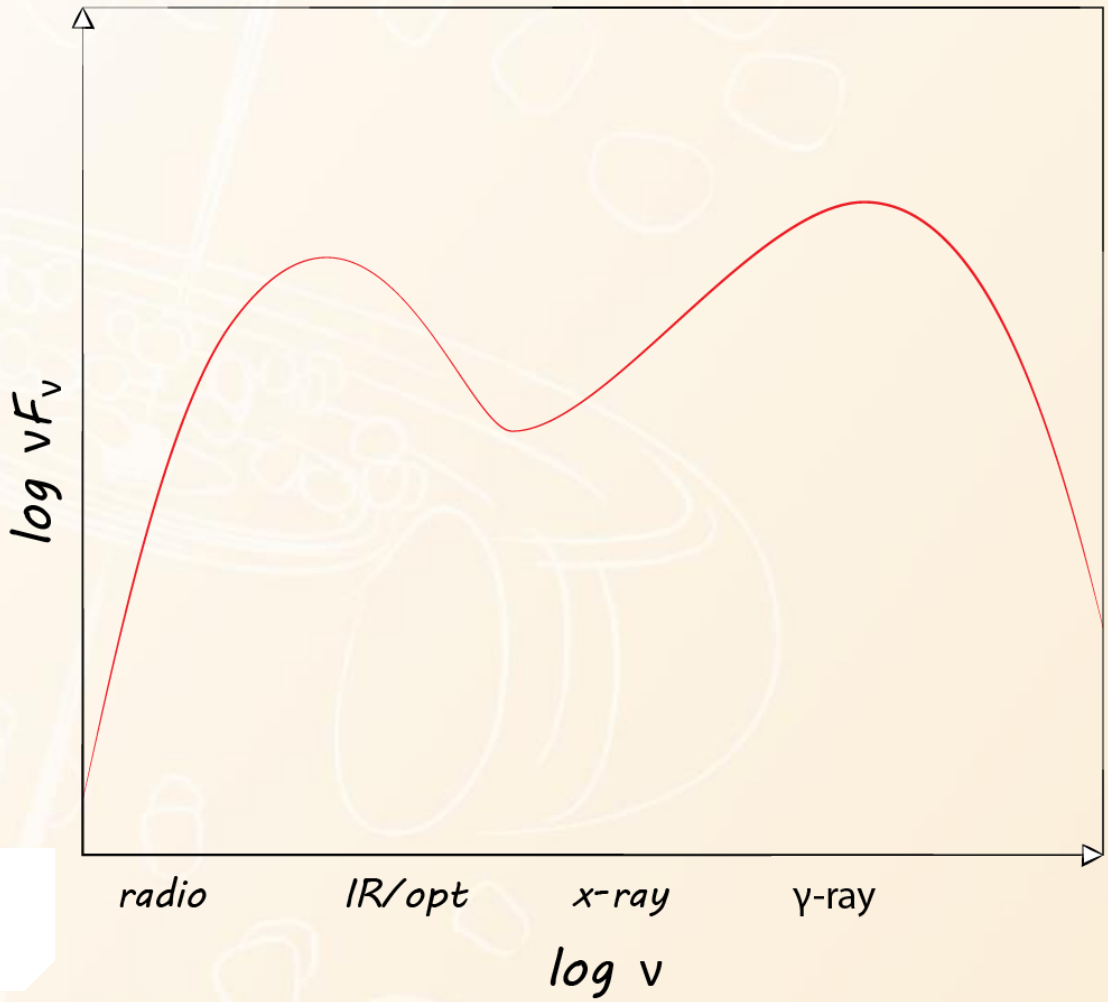

Fig. 2: Sketched spectral energy distributions of a blazar

I. Introduction:

EVPA swings

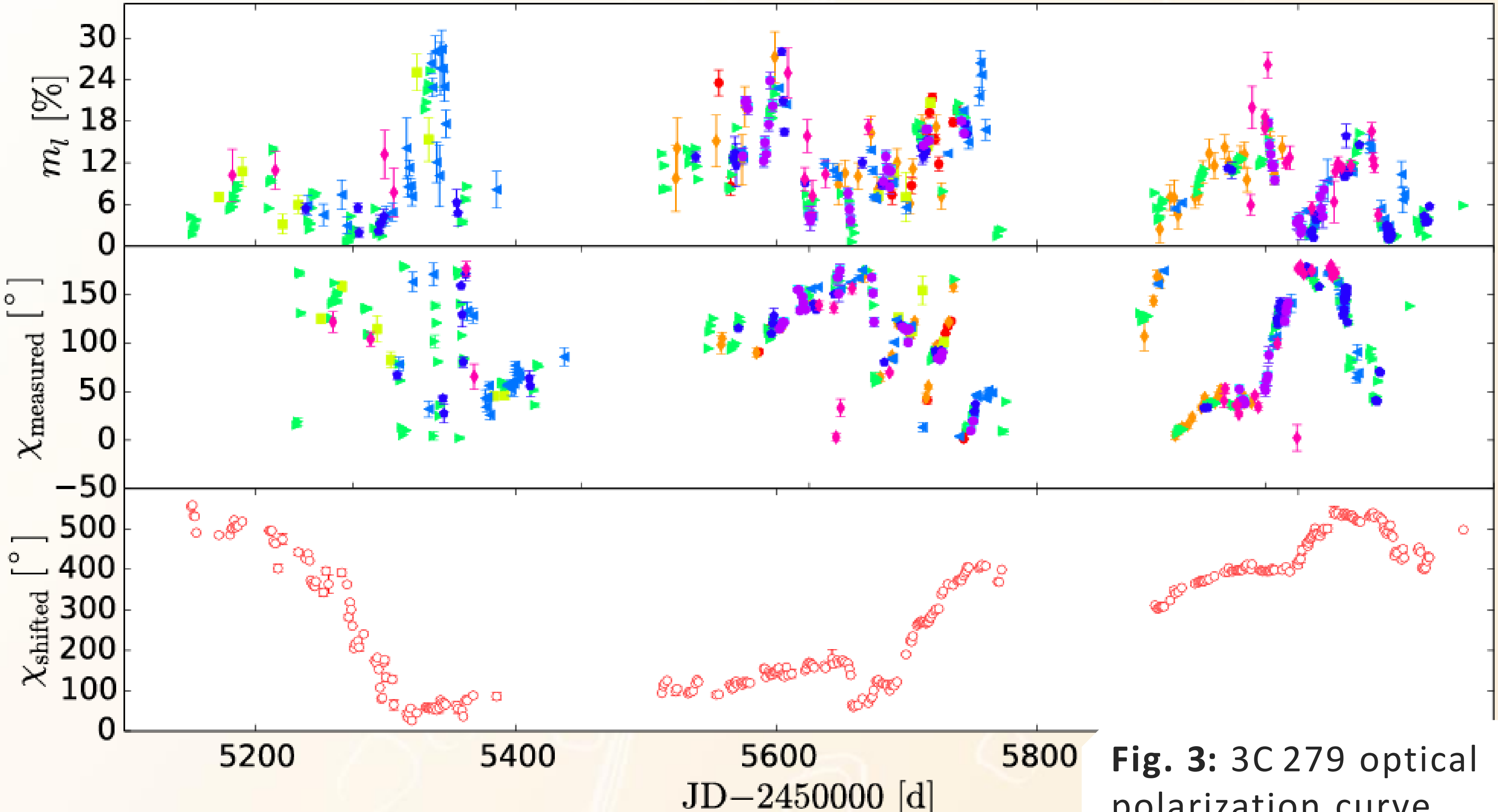

Fig. 3: 3C 279 optical polarization curve

I. Introduction:

EVPA swings

object	EVPA rotation	time interval	explanation	reference
OJ 287	120 °	7 d	Helical magnetic field	Kikuchi et al., 1988
BL Lac	240 °	5 d	Helical magnetic field	Marscher et al., 2008
PKS 1510+089	720 °	50 d	Helical magnetic field	Marscher et al., 2010
3C 279	↺ 300 °	60 d	Helical magnetic field	Larionov et al., 2008
3C 279	↻ 208 °	12 d	Bent jet	Abdo et al., 2010

II. Random walk:

randomized Stokes parameters

For each cell $i \in [1, N]$:

$$q_i = \mathcal{U}(-1, +1)$$
$$u_i = \mathcal{U}(-1, +1)$$

$$Q_i = \frac{q_i}{\sqrt{q_i^2 + u_i^2}} \cdot m_{l,\mathrm{max}}$$

$$U_i = \frac{u_i}{\sqrt{q_i^2 + u_i^2}} \cdot m_{l,\mathrm{max}}$$

$$m_{l,\mathrm{max}} = 75\ \%$$

Fig. 5.1

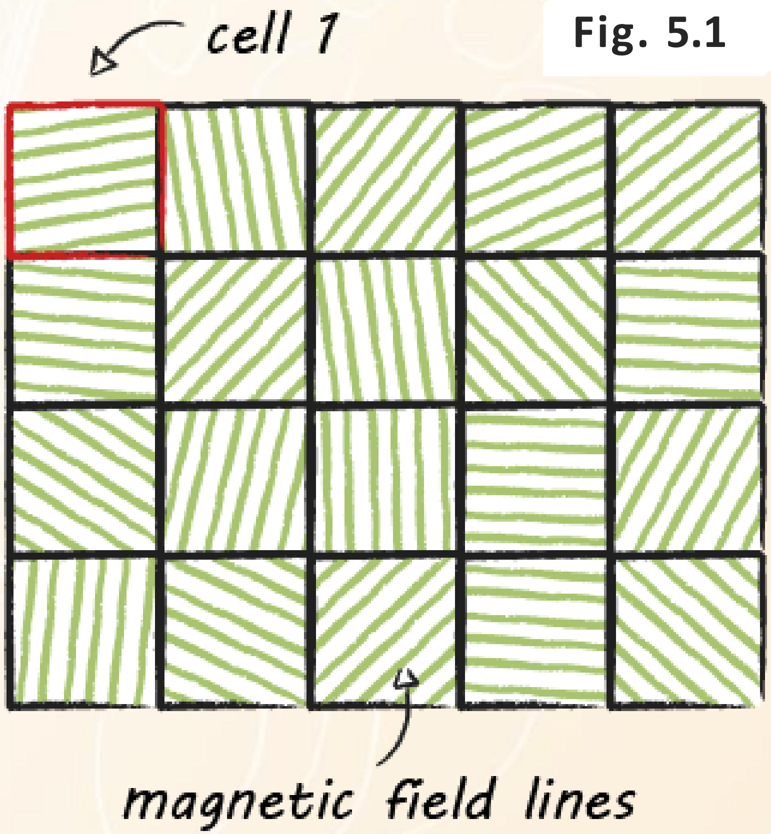

T.W. Jones et al. 1985, ApJ

F. D'Arcangelo et al. 2007, ApJ

II. Random walk:

simple and shock RW process

Simple random walk process:

Fig. 5.2

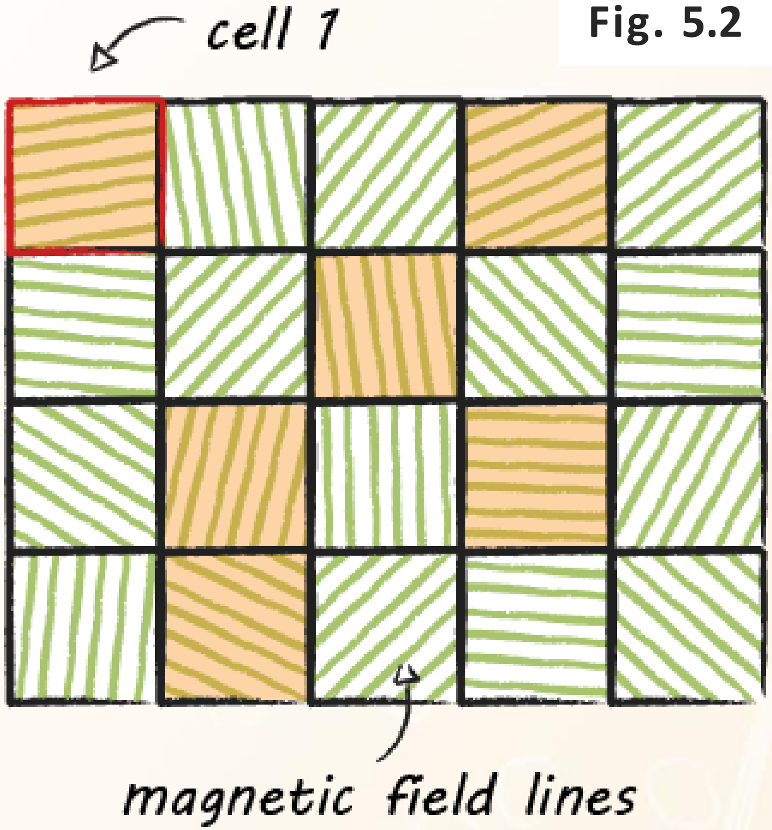

Shock random walk process:

Fig. 6

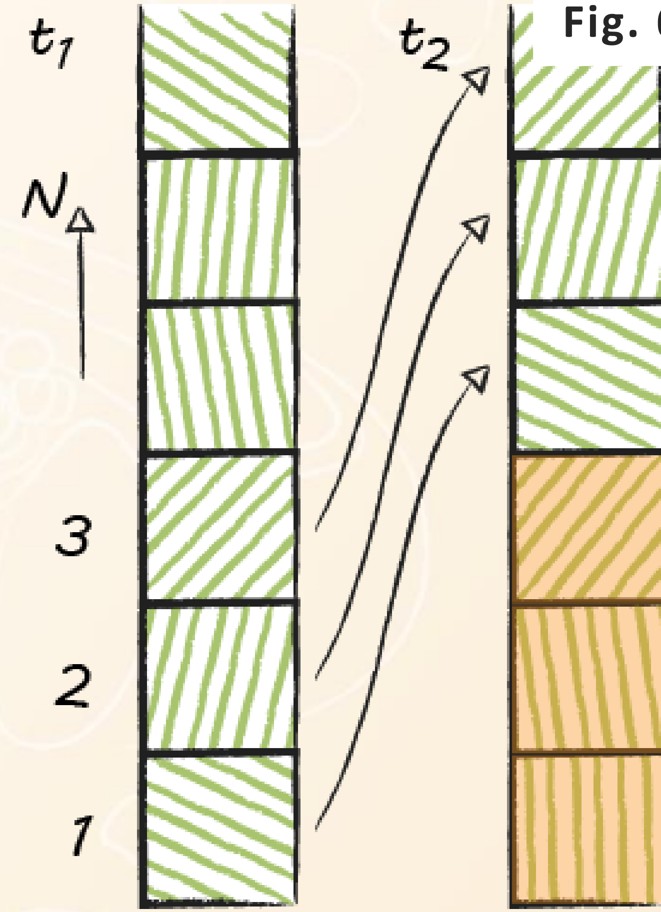

II. Random walk: parameters

Cells: N_{cells}

$$\langle m_l \rangle = m_{l,\max} \cdot \sqrt{\frac{\pi}{4N_{\text{cells}}}}$$

Variation rate: $n_{\text{var}}\ [\text{d}^{-1}]$

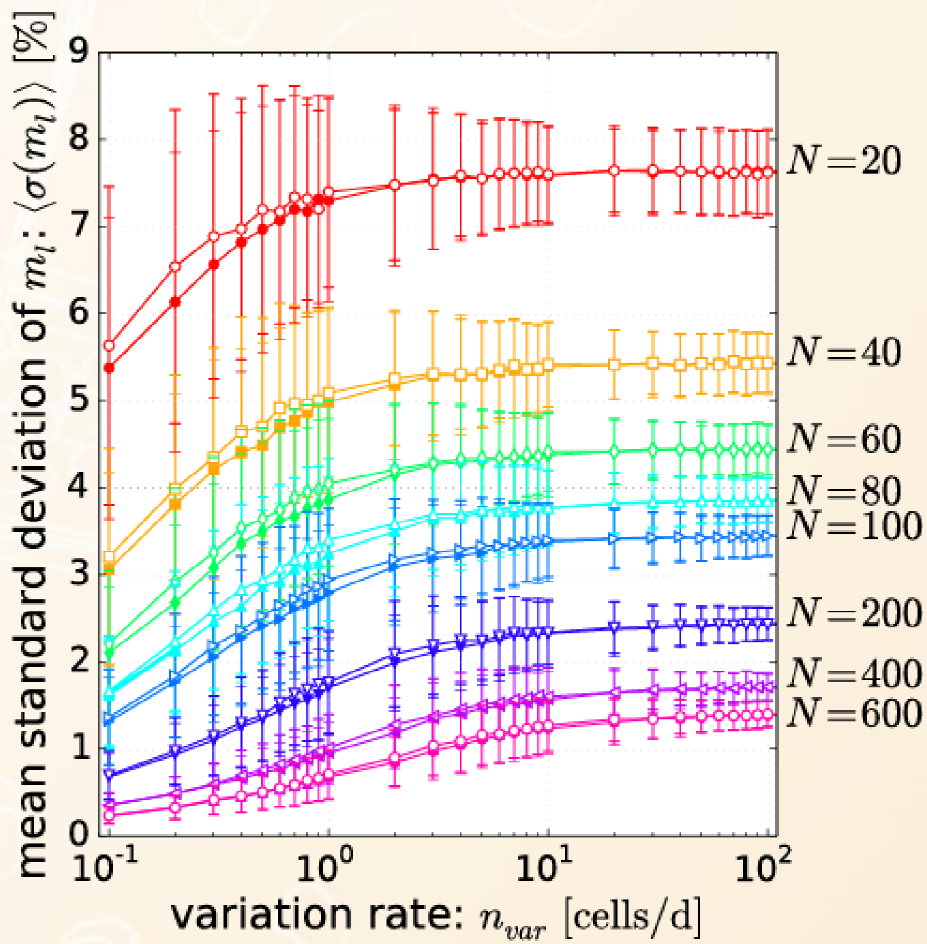

Fig. 7: Random walk processes: expectation value of the polarization fraction variation

II. Random walk: parameters

Vary:	N_{cells}	Number of cells
	n_{var}	Variation rate
Measure:	$\langle m_l \rangle$	Polarization mean
	$\sigma(m_l)$	Polarization variation
	$\Delta\chi$	EVPA swing amplitude
	s	Variation estimator
	N	Shifting consistency

III. Stochastic vs. deterministic:

3C 279 polarization

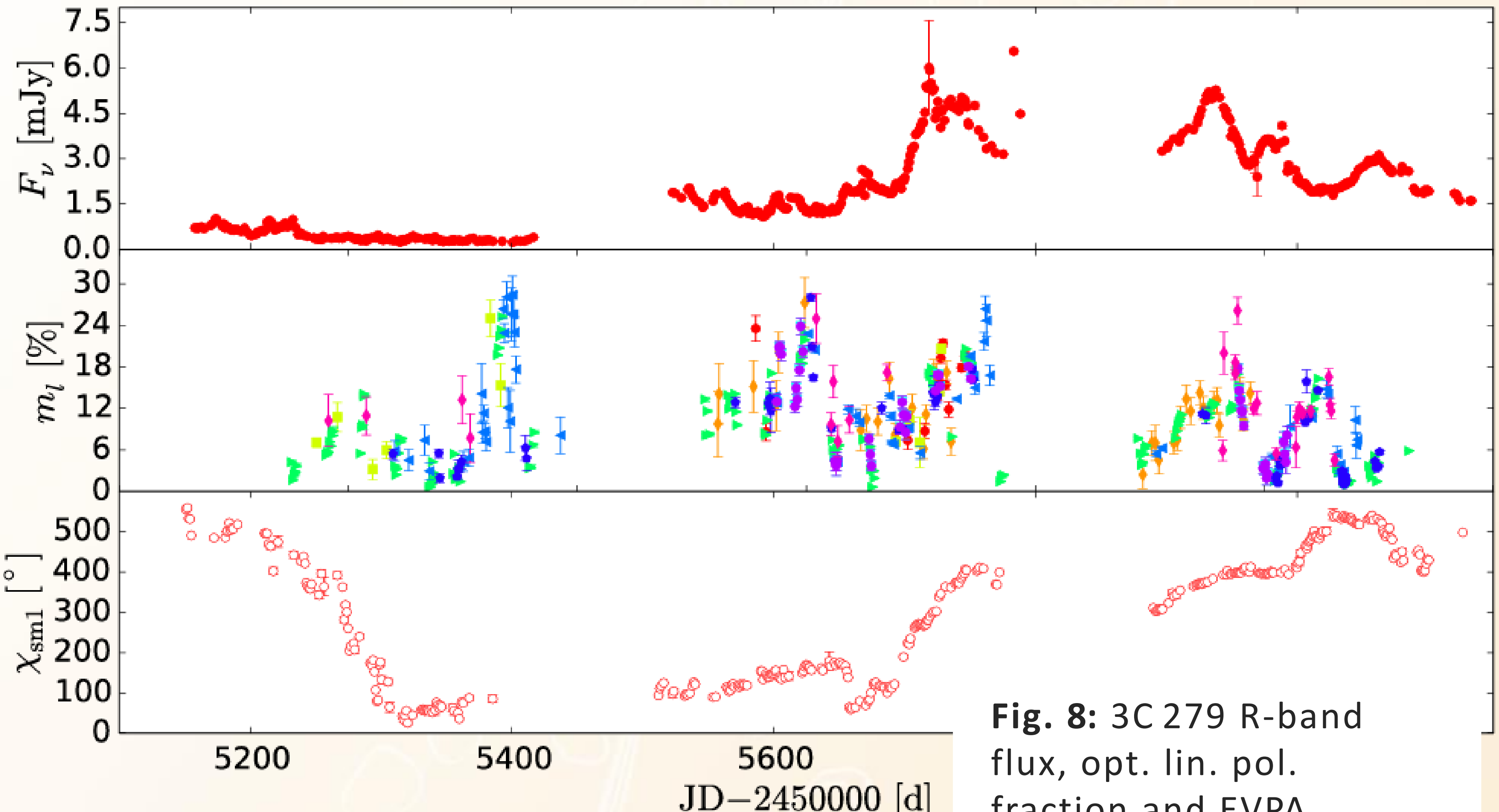

Fig. 8: 3C 279 R-band flux, opt. lin. pol. fraction and EVPA

IV. **EVPA swing mechanisms:**
Thick-to-thin-transition

Optically thick to optically thin transition
in radio, not in optical

Swing amplitude: $\Delta\chi = 90°$

for details: Ioannis Myserlis presentation

IV. EVPA swing mechanisms: Two/multi-component model

Ref.: Holmes et al. 1984, MNRAS

Swing amplitude:

$$\Delta\chi \leq 90°$$

Fig. 4: Two-component polarization curve

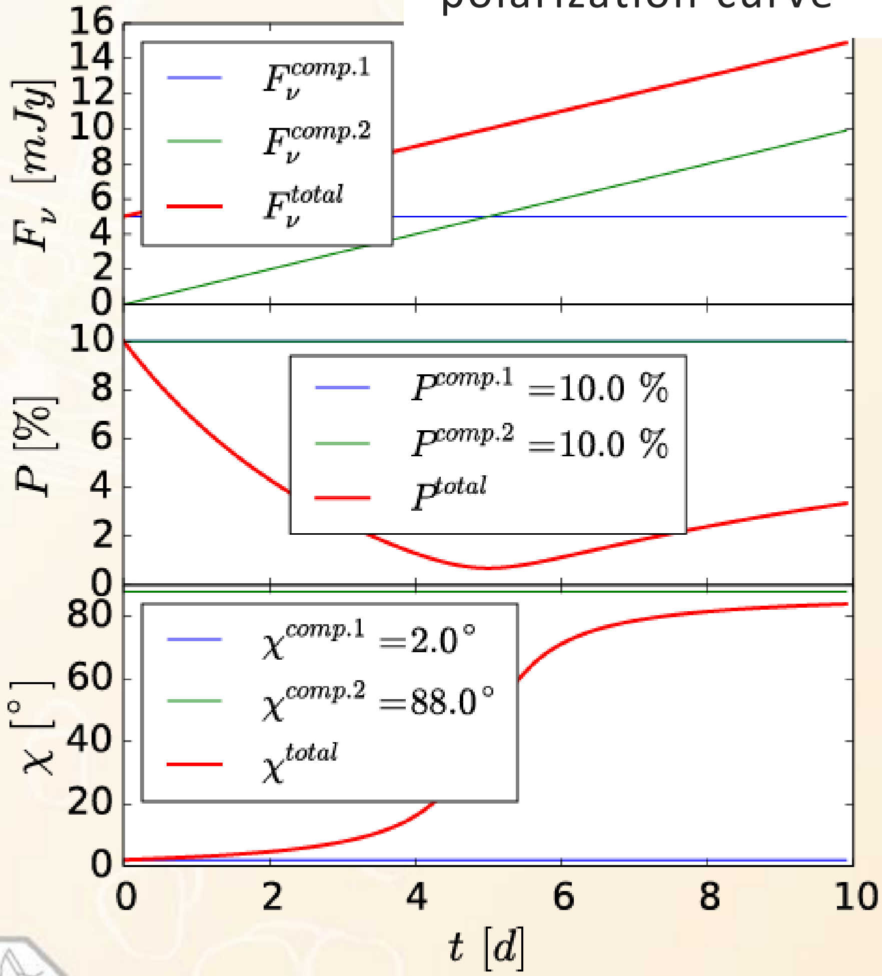

IV. EVPA swing mechanisms:

Bent trajectory

Ref.: Nalewaiko, 2012, IJMPD

e.g. bent jet

Swing amplitude:

$$\Delta\chi \lesssim 180°$$

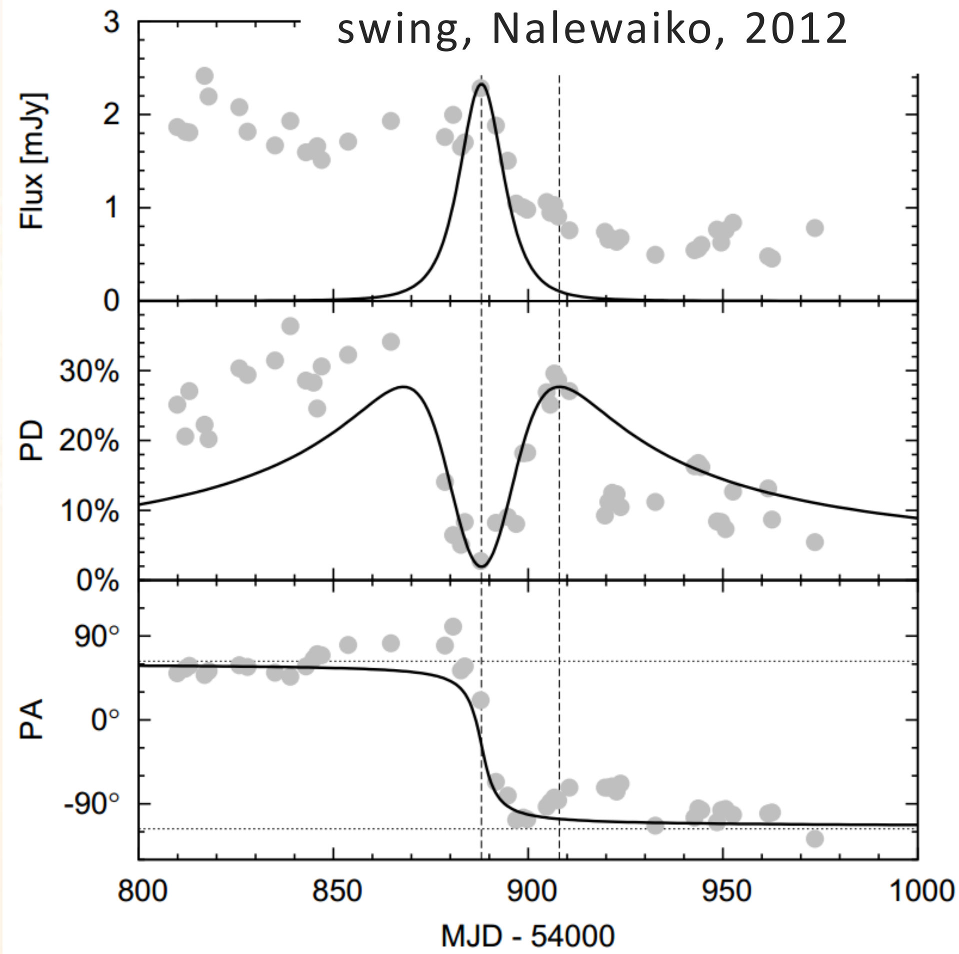

Fig. 5: Bent trajectory EVPA swing, Nalewaiko, 2012

IV. EVPA swing mechanisms:

Helical motion

Ref.: e.g. Marscher et al., 2008, Nature

Helical motion of an emission feature in a helical magnetic field

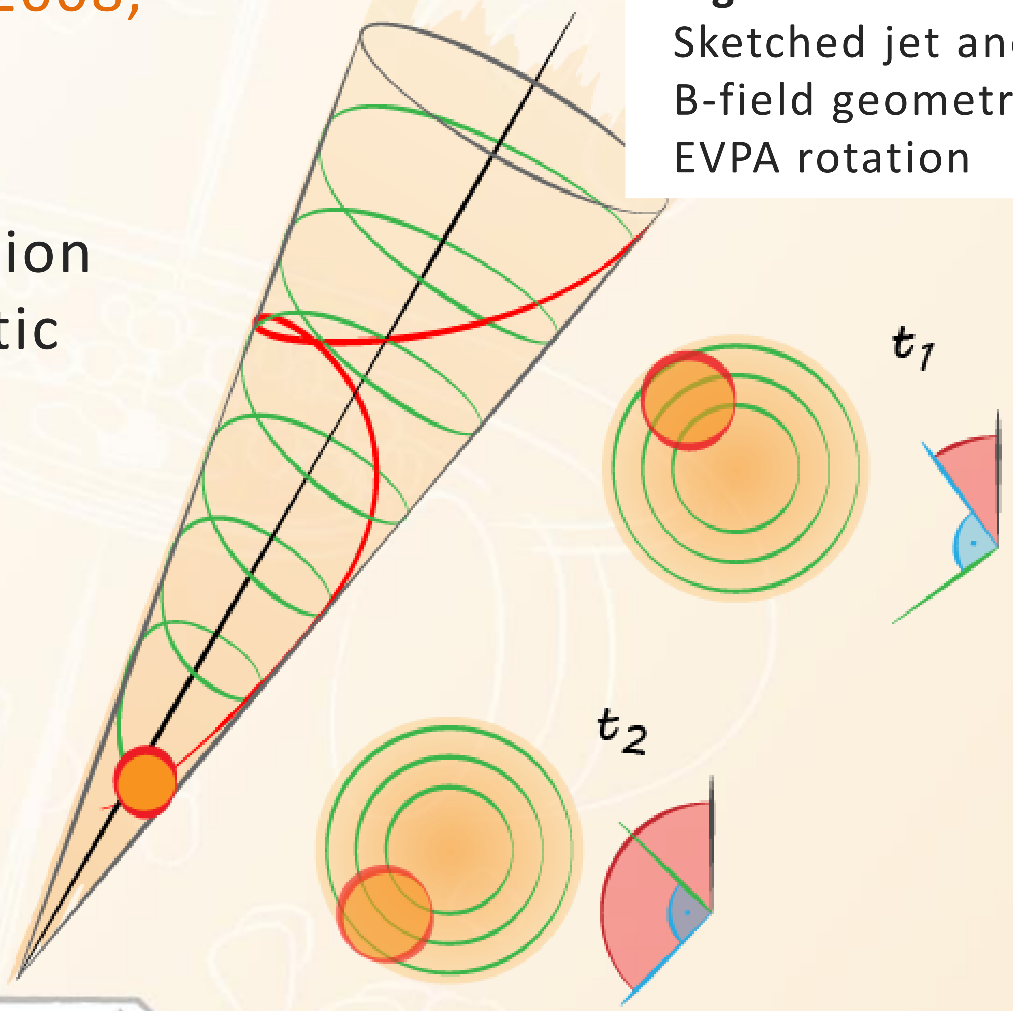

Fig. 6.1: Sketched jet and B-field geometry, EVPA rotation

v. Helical motion model: parameters

Motion and geometric parameters:		
Acceleration	a/c	$[d^{-1}]$
Begin acceleration zone	z_{ba}	$[R_S]$
End acceleration zone	z_{ea}	$[R_S]$
Downstream Lorentz factor	$\Gamma_{z,0}$	
Initial angular velocity	ϖ_0	$[°/d]$
Initial radial position	r_0	$[R_S]$
Initial angular position	φ_0	$[°]$
Opening index	$\rho \leq 1$	
Opening offset	z_0	$[R_S]$
Viewing angle	θ	$[°]$
Jet angle	η	$[°]$
Magnetic field parameters:		
Magn. field pitch angle	b	$[°]$
Component intrinsic flux density:		
Intr. flux density	f_ν^{intr}	[mJy]
Spectral index	$\alpha = 0.7$	

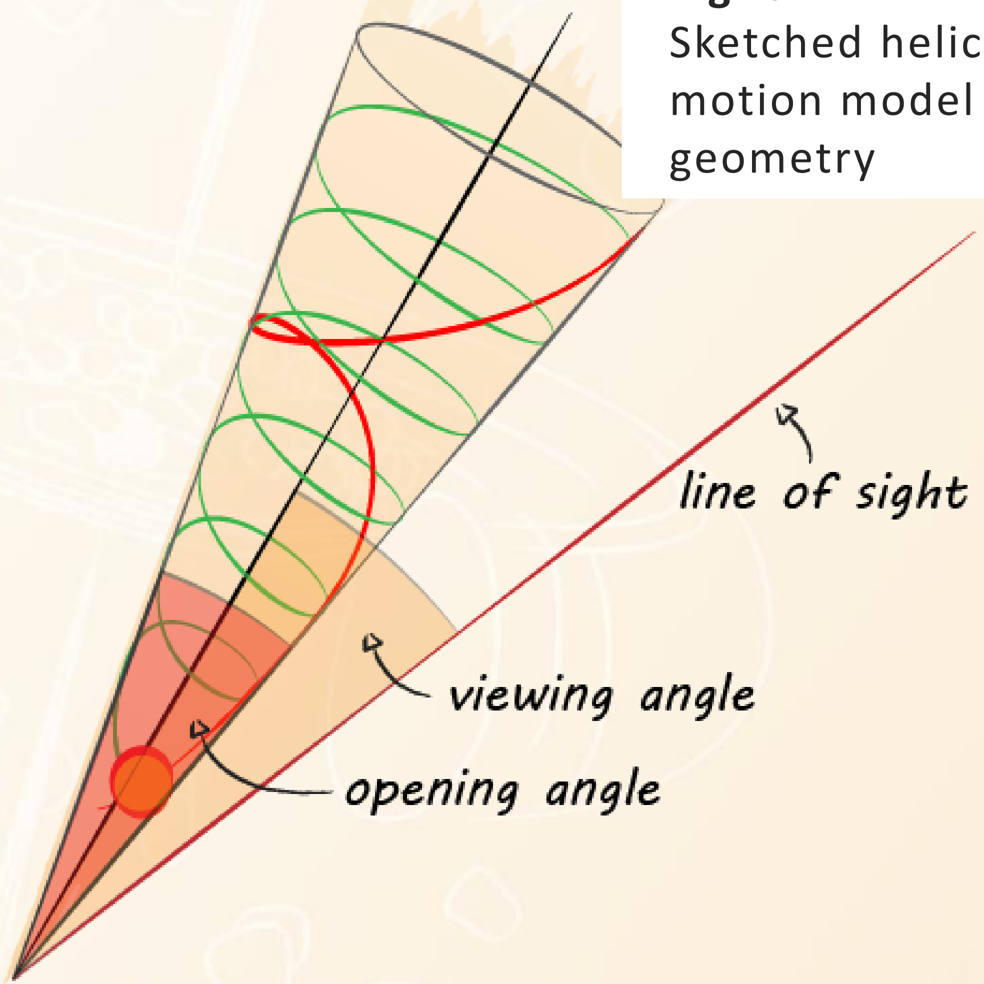

Fig. 6.2: Sketched helical motion model geometry

v. Helical motion model:

Single component

No acceleration.
Const. z-Lorentz factor Γ_z: 2.10
Initial angular velocity ω_0: 3.00 °/d
Initial z-position z_0: 0.00 R_S
Initial radial position R_0: 8.00 R_S
Initial angular position φ_0: 0.00 °
Opening index ρ: 0.40
Opening offset $z_{\rm off}$: 20.00 R_S
Viewing angle θ: 4.00 °
Jet angle η: 0.00 °
Magn. field pitch angle β: 70.00 °

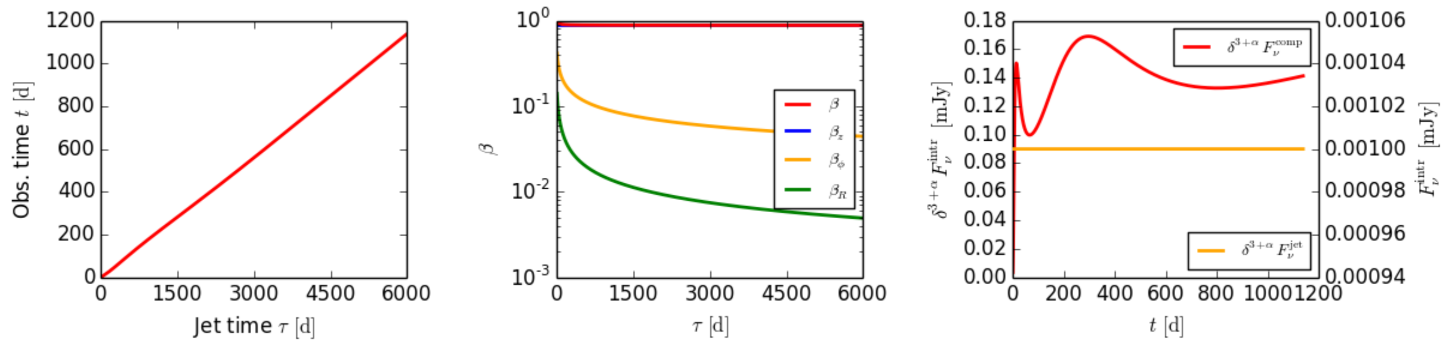

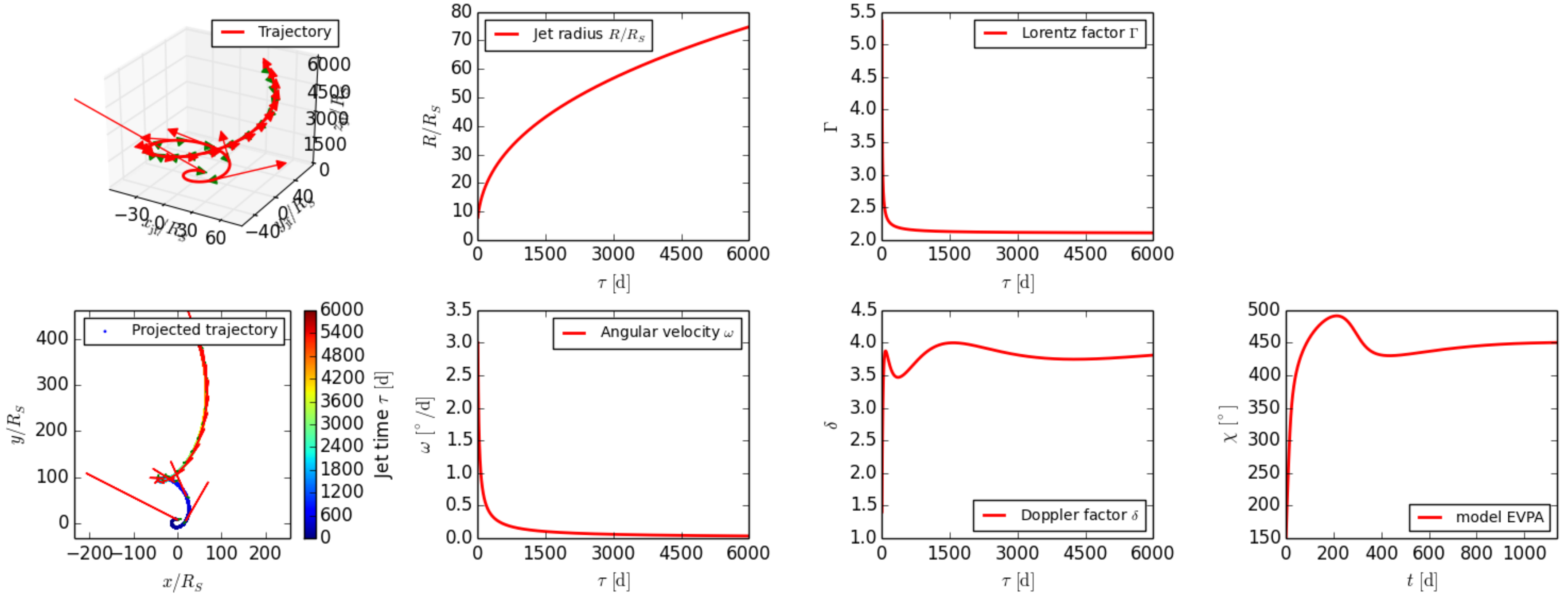

v. Helical motion model: parameters

Motion and geometric parameters:		
Acceleration	a/c	$[d^{-1}]$
Begin acceleration zone	z_{ba}	$[R_S]$
End acceleration zone	z_{ea}	$[R_S]$
Downstream Lorentz factor	$\Gamma_{z,0}$	
Initial angular velocity	ϖ_0	$[°/d]$
Initial radial position	r_0	$[R_S]$
Initial angular position	φ_0	$[°]$
Opening index	$\rho \leq 1$	
Opening offset	z_0	$[R_S]$
Viewing angle	θ	$[°]$
Jet angle	η	$[°]$
Magnetic field parameters:		
Magn. field pitch angle	b	$[°]$
Component intrinsic flux density:		
Intr. flux density	f_ν^{intr}	$[mJy]$
Spectral index	$\alpha = 0.7$	

Angular momentum conservation

Relativistic aberration

Time dilation: cosmological, motion

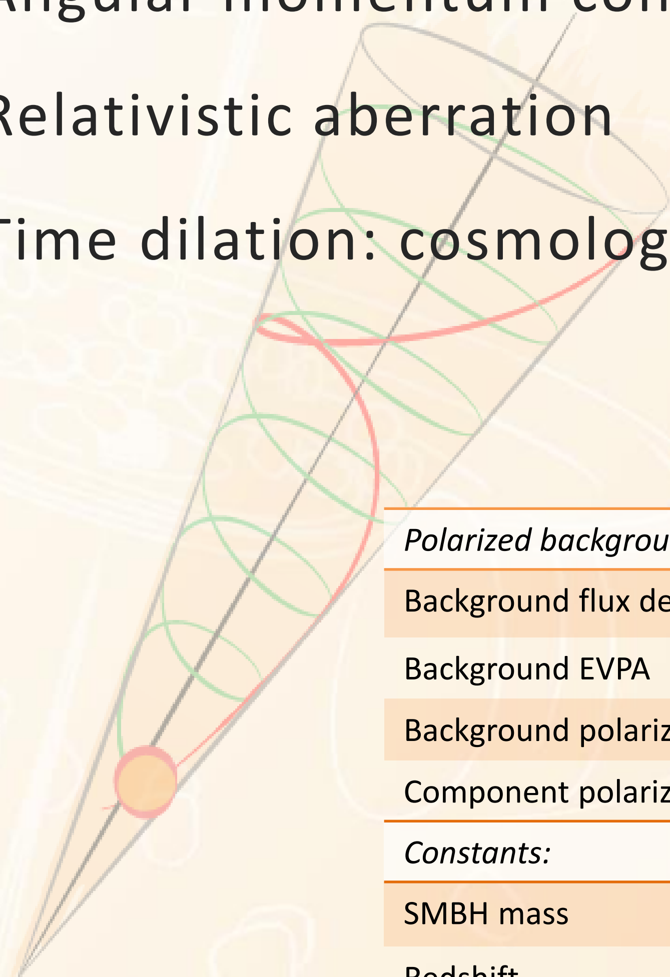

Polarized background:		
Background flux density	f_ν^{bg}	$[mJy]$
Background EVPA	χ^{bg}	$[°]$
Background polarization	P^{bg}	$[\%]$
Component polarization	P^{comp}	$[\%]$
Constants:		
SMBH mass	$M_{SMBH} = 8.6 \cdot 10^9 M_\odot$	
Redshift	$z = 0.5362$	

v. Helical motion model:

Single component + background

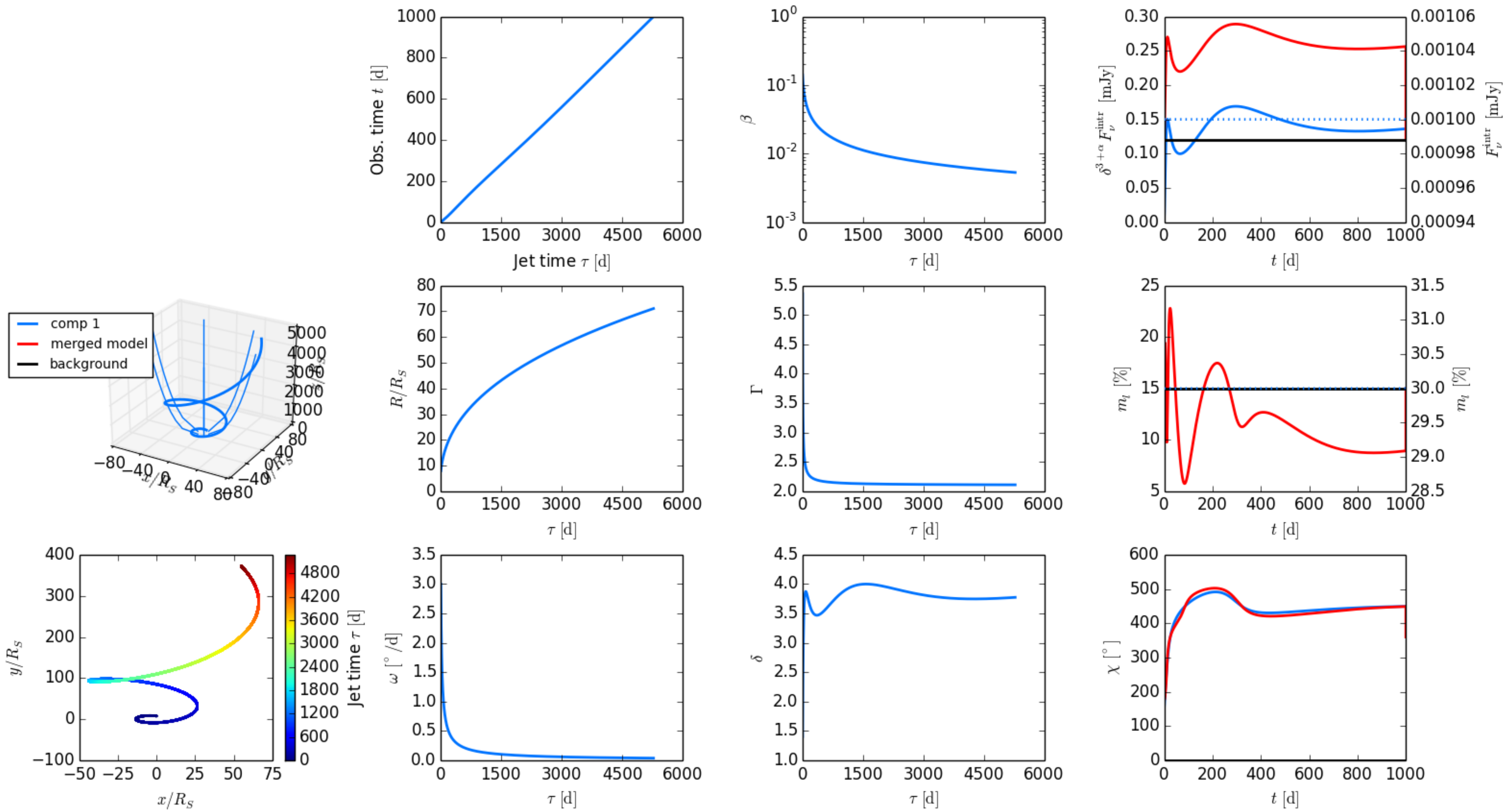

Conclusions

Random walks:

- 3C 279: two EVPA rotation processes
  - Low-state: stochastic variation
  - Flaring state: deterministic variation

Helical motion in helical magnetic field model:

- Can explain two-directional EVPA swings as observed in 3C 279

The Quasar Movie Project

Special thanks to the QMP collaborators:

T. Savolainen (PI), S.G. Jorstad, F. Schinzel, K.V. Sokolovski, I. Agudo, M. Aller, I. Berdnikov, V. Chavushyan, L. Fuhrmann, M. Gurwell, R. Itoh, J. Heidt, Y.Y. Kovalev, T. Krajci, O. Kurtanidze, A. Lähteenmäki , V.M. Larionov , J. León-Tavares, A.P. Marscher, K. Nilson, the AAVSO, the Yale SMARTS project and all the observers.

Acknowledgements:

SK was supported for this research through a stipend from the International Max Planck Research School (IMPRS) for Astronomy and Astrophysics at the Max Planck Institute for Radio Astronomy in cooperation with the Universities of Bonn and Cologne.

Data from the Steward Observatory spectropolarimetric monitoring project were used. This program is supported by Fermi Guest Investigator grants NNX08AW56G, NNX09AU10G, and NNX12AO93G.

We acknowledge with thanks the variable star observations from the AAVSO International Database contributed by observers worldwide and used in this research.

MAX-PLANCK-GESELLSCHAFT

IMPRS astronomy & astrophysics Bonn and Cologne

Appendix

A. nπ-ambiguity:

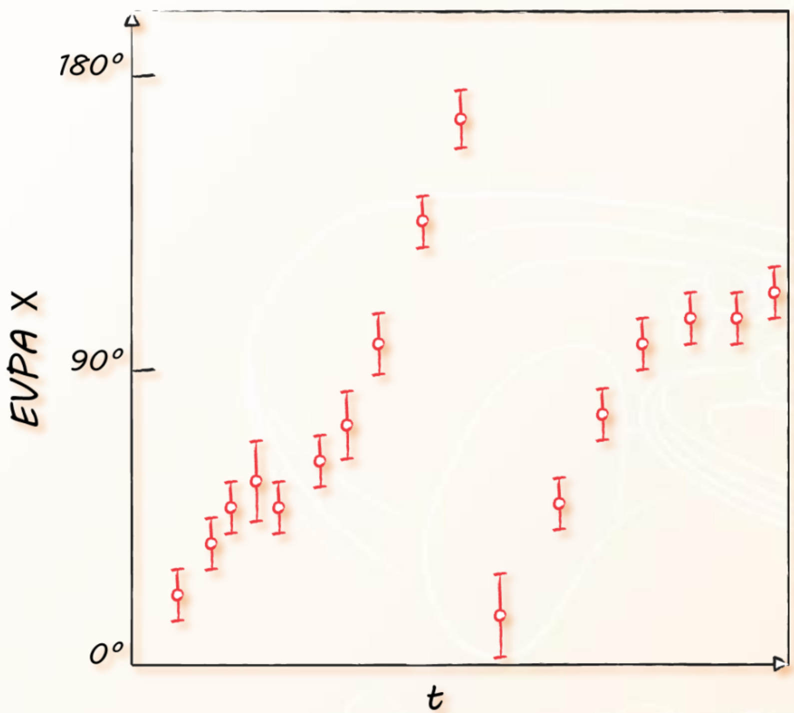

Fig. 1.1: Sketched EVPA curve

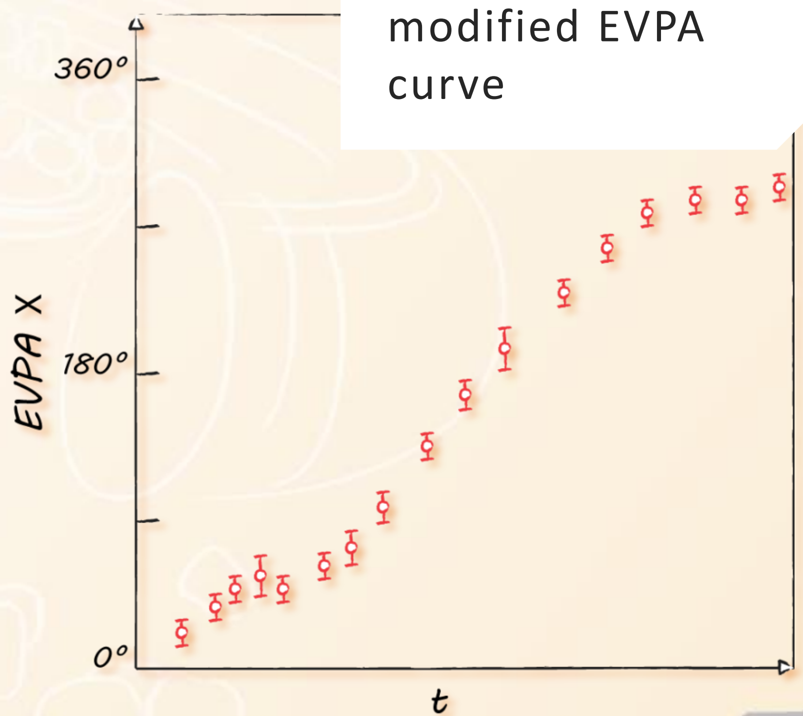

Fig. 1.2: Sketched modified EVPA curve

Appendix

A. nπ-ambiguity: Shifting methods

Method 1:

Fig. 2.1

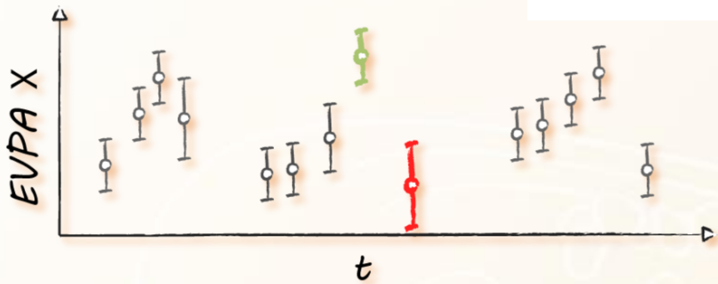

$$\Delta X_i = |X_i - X_{i-1}| - \sqrt{\sigma^2(X_i) + \sigma^2(X_{i-1})}$$

if $\Delta X_i > 90°$

Method 2:

Fig. 2.2

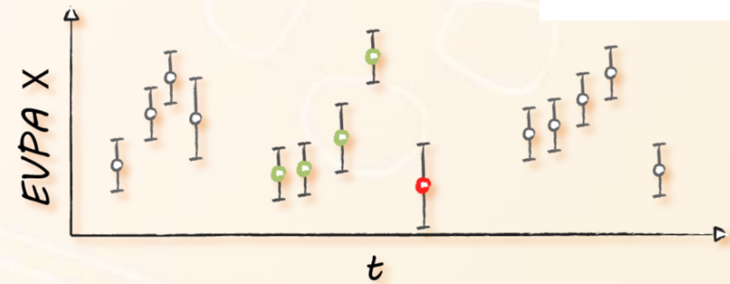

$$X_{ref,i} = \langle [X_{i-1-N}, X_{i-1}] \rangle$$

$$N = 1, 2, 3, \ldots$$

if $|X_i - X_{ref,i}| > 90°$

$$X_{mod,i} = X_i \pm n \cdot 180°$$

Appendix

A. nπ-ambiguity: Shifting consistency

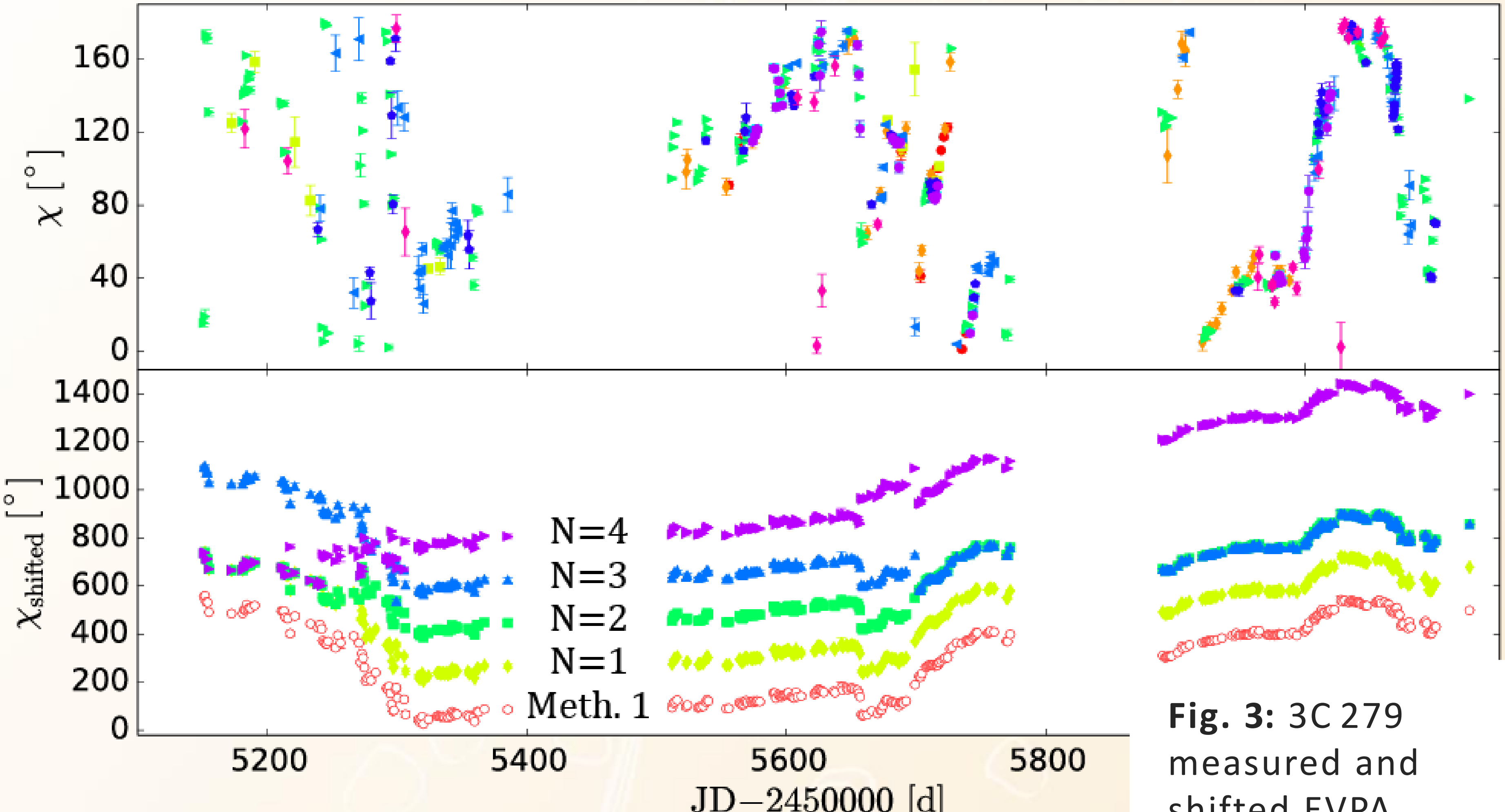

Fig. 3: 3C 279 measured and shifted EVPA

Appendix

B. Curve smoothness:

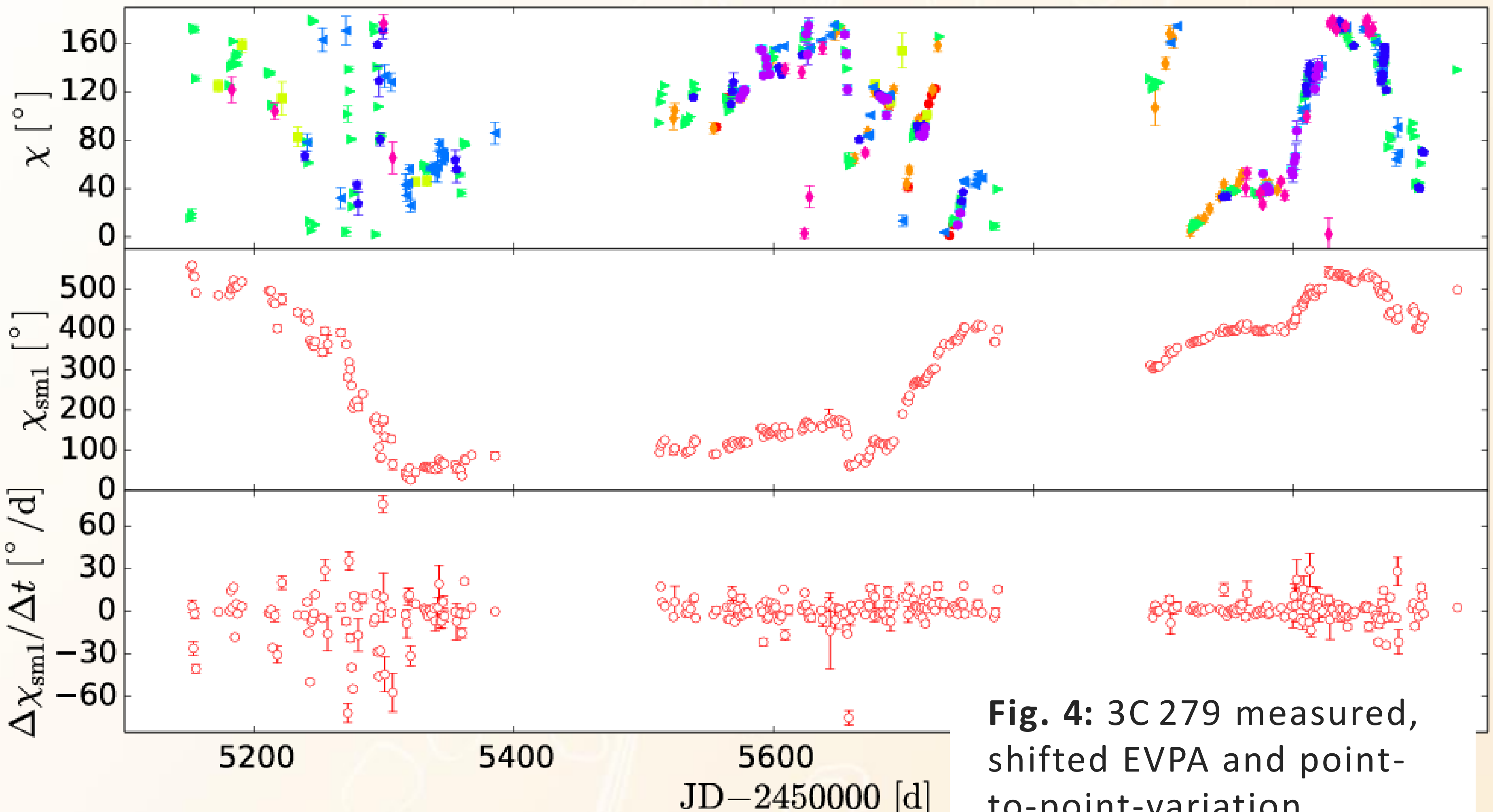

Fig. 4: 3C 279 measured, shifted EVPA and point-to-point-variation

B. Curve smoothness: Variation estimator

Point-to-point variation: $\left(\frac{\Delta X}{\Delta t}\right)_i = \frac{X_i - X_{i-1}}{t_i - t_{i-1}}$

Tendency: $m = \left\langle \left(\frac{\Delta X}{\Delta t}\right)_i \right\rangle$

Variation estimator: $s = \left\langle \left| \left(\frac{\Delta X}{\Delta t}\right)_i - m \right| \right\rangle$

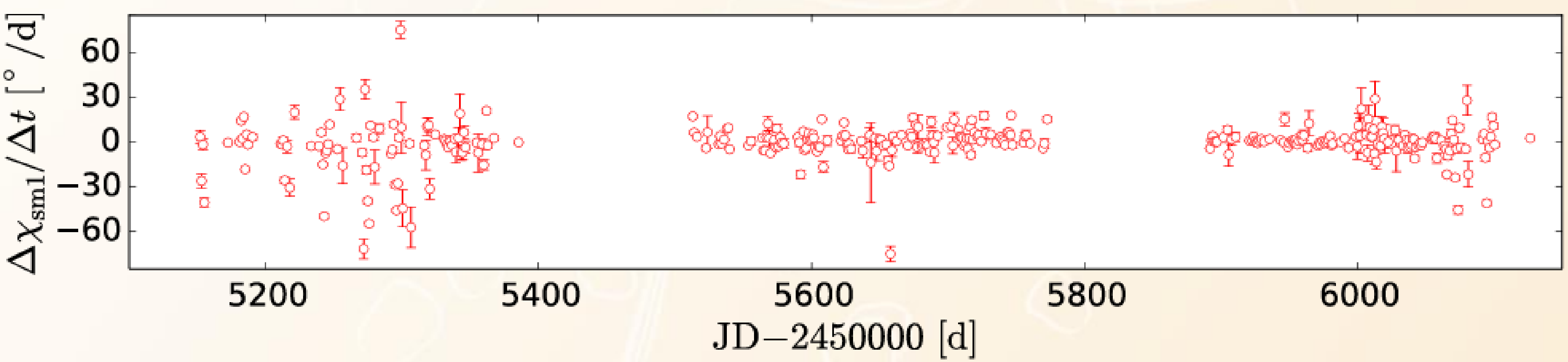

Appendix

B. Curve smoothness: Variation estimator

$s = 14.1(8)\ °/\text{d}$ $s = 5.7(5)°/\text{d}$ $s = 5.5(5)°/\text{d}$